ORIGINAL ARTICLE

CrossMark

Observations of in vivo laser tissue ablation in animal models with different chromophores on the skin and modulating duration per laser exposure

Hang Chan Jo[1,2] · Dae Yu Kim[1,2]

Abstract
Characteristics such as skin tone and pigmentation color vary among patients, but most researches on laser irradiation in laser ablation have revolved around minimizing damage to reduce pain. Chromophores are the most important factors in photon energy absorption, a key principle of laser ablation. We investigated the influences on ablation depth by different chromophores on the target and modulating duration per laser exposure using an Nd:YVO4 nanosecond 532-nm laser. We used a Fourier-domain optical coherence tomography (Fd-OCT) system combined with a 532-nm Nd:YVO4 laser to observe the ablation process. In addition, an external customized shutter and water-based color pens (red, green, blue, black) were used to determine the effects of modulating the duration per laser exposure and coloring chromophores on porcine skin and hairless mouse models. Experiments with modulating duration per laser exposure demonstrated that shorter duration generated shallower craters than longer one. Painted experimental group showed damaged region as craters in the experiments with coloring various chromophores. In this research, we investigated the effects of modulating duration per laser exposure and different chromophores on the target. Coloring chromophores with water-based dyes using pens increased tissue damage without dyeing cells or tissue.

Keywords 532-nm laser · Laser ablation · Laser exposure conditions · Shutter on-off frequency modulation · Duration per laser exposure · Fd-OCT · OCT monitoring · Ablation monitoring

Introduction

Laser ablation is a method of removing materials from a target surface via the photothermal effect of a focused laser beam and energy absorption [1]. It is currently applied in various industrial processes and the medical fields. Laser surgical procedures are especially popular tools in dermatology, cardiology, dentistry, oncology, and ophthalmology [2–9]. Ablation treatments in dermatology are routinely used to treat pigmentation disorders [10, 11]. Dermatology patients experience different levels of pain during laser treatments under the same laser conditions because of individual characteristics such as skin tone, pigmentation levels, and chromophores. Previous researches have focused on minimizing marginal damage and enhancing ablation efficiency under various laser conditions [12–16]. Correlations between ablation and pulse duration were investigated in earlier researches on laser ablation using the Er:YAG laser and pulsed CO2 laser through photomicrographs of punch biopsy samples collected under light microscopy [12–16]. These papers showed that long pulse irradiation created larger marginal damage zones than short pulse irradiation [12–16]. Although correlations between ablation and laser conditions have been demonstrated in several previous studies [17, 18], the effect of tissue color on ablation has not been reported. Moreover, specific skin color criteria for laser irradiation do not exist, although patient pigmentation colors and skin tones vary widely. The development of laser treatment standards for dermatology could potentially mitigate side effects in patients undergoing such procedures and surgeries.

Optical coherence tomography (OCT), which is a noninvasive imaging technology for biological tissue, can be used to observe ablation [19]. OCT is a noninvasive optical imaging

✉ Dae Yu Kim
dyukim@inha.ac.kr

1   Bioelectrical Engineering Lab, Electrical Engineering, Inha University, 100 Inha-ro, Michuhol-gu, Incheon 22212, South Korea

2   Electrical Engineering, Inha University, 100 Inha-ro, Michuhol-gu, Incheon 22212, South Korea

method based on the Michelson interferometer using superluminescent diodes [20]. OCT systems are used for various medical applications including OCT biopsy, OCT angiography, endoscopic OCT, spectroscopic OCT, and blood flow OCT [20–28]. OCT can be used to obtain micro-unit images of two-dimensional (2D) and three-dimensional (3D) depth through laser scanning. In particular, OCT can provide accurate cross-sectional depth images, which allow observation of ablation craters.

In this paper, we report the effects of laser tissue ablation according to different chromophores on the skin and modulated shutter on-off frequency as a step toward developing criteria for accurate laser irradiation in dermatologic applications. Fourier-domain OCT was used to monitor ablation and a Nd:YVO4 532-nm nanosecond laser was used to irradiate laser on the target. The OCT beam (central wavelength of 860 nm) and the ablation laser beam (532 nm) were combined for monitoring via a dichroic mirror. The objective lens used in these experiments was an achromatic doublet lens (AC254-030-B-ML, Thorlabs, Newton, NJ, USA) available for 532-nm and 860-nm beams. Various laser exposure conditions were controlled by modulating shutter on-off frequency by a customized external shutter. Additionally, various colors were painted on the skin using water-based pens.

Materials and methods

Monitoring system

To observe ablation of the tissue surface, Fourier-domain optical coherence tomography (Fd-OCT) and a 532-nm Nd:YVO4 laser were combined on the sample arm using a dichroic beam splitter (FF662-FDi01-25 × 36, Semrock, Rochester, NY, USA) and an objective lens. A schematic design of the system is shown in Fig. 1. The light source was a superluminescent diode (T860-HP, SUPERLUM, Carrigtwohill, Ireland, central wavelength = 860 nm, bandwidth = 135 nm, output power = 3 mW) and was combined with an optical isolator. In this system, the lateral resolution was approximately 10 μm and the axial resolution was approximately 5 μm. Each B scan consisted of 440 axial scanning (A-scans) with a 20-kHz scanning rate on the sample. The beam-splitting fiber coupler (AC Photonics, Santa Clara, CA, USA) had a 50/50 ratio. To build the spectrometer, a 1200 L/m+ m diffraction grating (Wasatch Photonics, Durham, NC, USA), a 150-mm objective lens and a 12-bit line scan camera (spL4096–140 km, Basler AG, Ahrensburg, Germany) were used. Laser scanning patterns were generated using a Galvo Scanner (8315 K, Cambridge Technology, Bedford, MA, USA) for the X–Y scan. Fringe patterns were acquired by a high-performance frame grabber (PCIE-1433, National Instruments, Austin, TX, USA)

through a line scan camera (active pixels: 2048). Data were processed using custom-built Fd-OCT software written in LabVIEW (National Instruments, Austin, TX, USA). The Q-switch diode-pumped Nd:YVO4 nanosecond laser was used to ablate samples. Specifications of the laser included a 15-ns pulse width at a 20-kHz repetition rate, 532-nm wavelength, and a 1.6-mm Gaussian beam diameter aperture.

Modulating the duration per laser exposure

Ablation is a phenomenon based on the photothermal effect, the outcomes of which vary depending on various sample characteristics and laser conditions. Previous studies investigated correlations between ablation and the pulse duration (laser "on" time, also known as pulse width) using Er:YAG and pulsed CO_2 lasers [12–16]. These studies showed that pulse duration affects ablation quantity and causes marginal damage. In their experiments, longer pulse irradiation resulted in wider and deeper craters than shorter irradiation. Although samples need the time called the thermal relaxation time to radiate heat, longer pulse irradiations accumulate energy on the sample continuously. The thermal relaxation time is defined as the time required for the target to dissipate approximately 63% of the absorbed energy [29, 30]. If the target tissue was heated over 45 °C by the laser, the thermal energy generated thermal damage including enzymatic changes, edema, coagulation, and vaporization on the tissue. Reducing heat accumulation by modulating laser duration could prevent the side effect of post-inflammatory hypopigmentation and hyperpigmentation (PIH) with minimal thermal ablation.

To verify previous researches on pulse duration, we conducted shutter on-off frequency modulation to change the duration per laser exposure. Here, the duration per laser exposure defines the time of laser exposure during a shutter opened. All external pulses for shutter on-off frequency modulation were operated with a 50% duty cycle. An external laser shutter (SHB1T, Thorlabs, Newton, NJ, USA) was customized through a transistor-transistor logic (TTL) signal from a microcontroller unit (MCU; Arduino Uno). We applied this customized external shutter [Fig. 2(a), (b)] to allow us to generate various laser exposure conditions using MCU firmware coding. This shutter system permitted trigger, pause statement, and repetition as well as modulating the laser exposure conditions via floating firmware codes. Shutter operation was delayed for 21 ms and the response time was decreased by 6 ms according to the input pulse signal. The minimum exposure time was 50 ms in our experiments. The delay time (until fully open) E–B was 21 ms, minimum drive pulse E–C was 25 ms, the delay time (the close start time) C–D was 15 ms, and the decreased exposure time was 6 ms = (E–B)–(C–D) as shown in Fig. 2c.
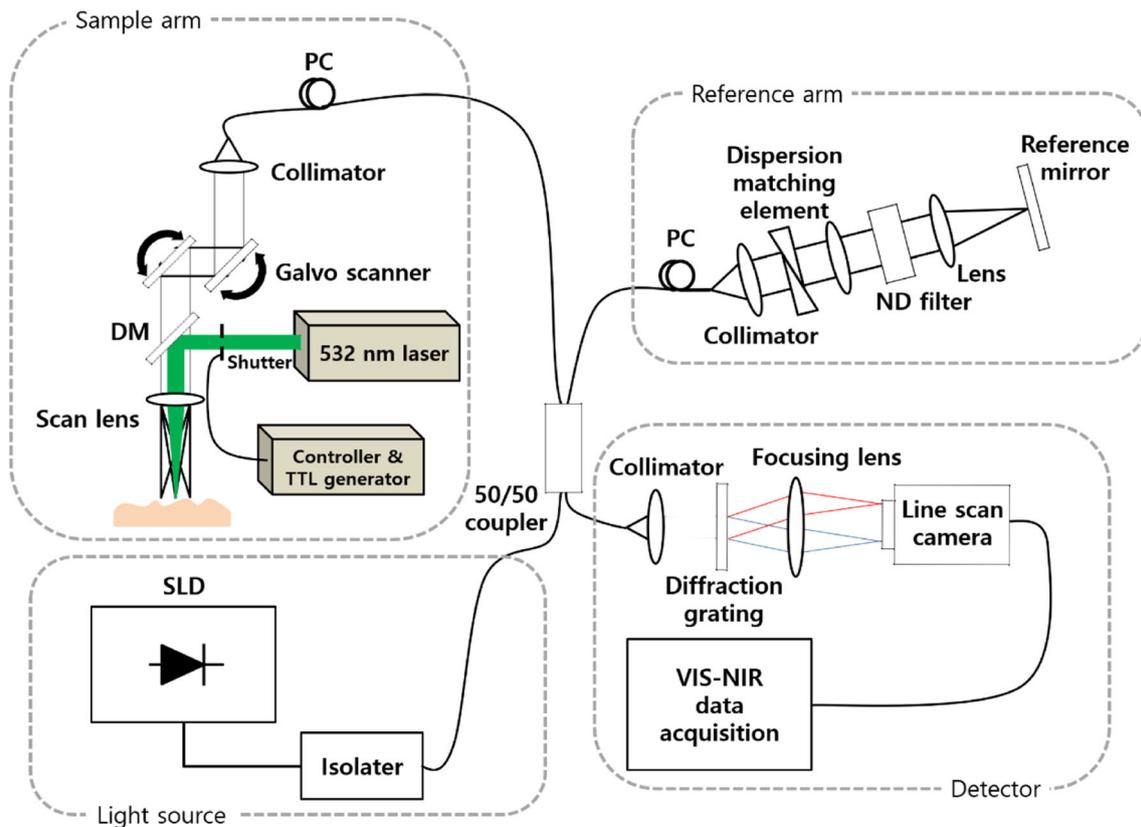
Fig. 1 A schematic image of the monitoring system. DM, dichroic mirror; PC, polarization controller; ND filter, neutral density filter. An OCT imaging system with an Nd:YVO4 laser with a wavelength of 532 nm was used. The laser beam for ablation was reflected by a dichroic mirror with > 95% reflection in the OCT laser path after the X–Y scanner (Galvo Scanner). A superluminescent diode (SLD) light source was operated at 3 mW and penetrated the dichroic mirror with <

7% loss. The light back-reflected from the sample and the reference mirror were combined in the fiber coupler. The interference pattern from the combined beam went to the spectrometer. Fringe patterns of integrated light were acquired by a line scan camera. Although this system permits linear scanning and 3D scanning via the X–Y scanner, only linear scanning was performed to obtain a fast response in this work

Different chromophores on the tissue

Chromophores, as absorbers of photon energy emitted from the laser, are important factors to consider when making use of the photothermal effect. These can exist in the form of melanin, pigment, and heme in the skin. Although water was one of the absorbers in this study, we ignored it as a light absorber because absorbance of water in 532 nm was insignificant according to the optical window [31]. To create experimental chromophore groups, four colored water–based pens (Plus pen 3000, MONAMI, Yongin, South Korea) were used. Black, red, green, and blue ink
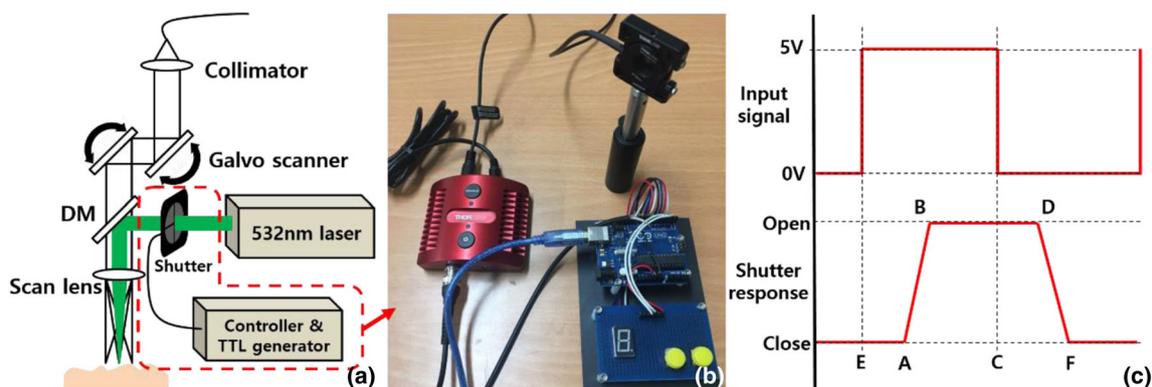

Fig. 2 a Schematic, **b** actual images, and **c** timing diagram of the customized external shutter. Arduino firmware created the transistor-transistor logic (TTL) square wave signal for the open-and-close motion of the shutter

Table 1 Colors painted on the sample surface

Color	C	M	Y	K	Color code
Red	C: 10	M: 100	Y: 100	K: 0	#E60000
Green	C: 100	M: 0	Y: 100	K: 0	#00FF00
Blue	C: 100	M: 75	Y: 0	K: 0	#0040FF
Black	C: 0	M: 0	Y: 0	K: 100	#000000

C cyan, *M* magenta, *Y* yellow, *K* black

were thinly colored on the sample surfaces. Table 1 shows the four colors of the water-based pens.

Materials in the ink included ethylene glycol (CAS no. 107-21-1), glycerine (CAS no. 56-81-5), water (CAS no. 7732-18-5), and components used as a dye. Each ingredient and their combination (ethylene glycol + glycerine, ethylene glycol + water, glycerine + water, ethylene glycol + glycerine + water) were tested to investigate chemical effects. None of the components or combinations influenced ablation except the dye.

Samples

For experiments, porcine skin and living hairless mouse were used in in vitro and in vivo experiments, respectively, as substitutes for human skin. Porcine skin is widely used as a human tissue substitute for percutaneous absorption tests [32].

Fresh, depilated porcine skin was obtained from a slaughterhouse. Hairless mouse (HR-1) used in the experiments were freshly depilated because of their downy hair and thin skin. To treat mouse and acquire data, an anesthetic mixture of Zoletil and Rompun was used. Experiments using hairless mouse were approved by the institutional animal care and use committee (IACUC) of Dankook University.

Results

We acquired OCT cross-sectional data from the surfaces of the samples. To acquire data, the Fd-OCT and laser were operated at the same beam path for ablation monitoring. The Nd:YVO4 laser operated in CW mode at a 532-nm wavelength was used to ablate samples under various irradiating conditions. The focused beam of the laser which could be operated at a maximum power of 4 W was modulated in each experiment. The focused beam radius was 0.8 mm and the beam propagation factor (M2) was 1.2. The linear scanning range of the Galvo scanner used in all experiments was 3.25 mm. To measure the depths of the craters, pixel (size 1.23 μm × 1.23 μm) numbers were counted from the surface of the tissue in the ablation state to the bottom of the craters. All images were immediately captured after laser irradiation.

Fig. 3 Ablation results for porcine skin obtained by modulating the duration per laser exposure. (**a**, **d**, and **g**) Images of the samples before laser irradiation. Each ablation was performed for a total of 12 s. The duration in each period for (**a** and **b**): 1 s. The duration in each period for (**d** and **e**): 2 s. The duration in each period for (**g** and **h**): 3 s. The duty cycles of all periods were 50%. Laser beam power was 350 mW. The yellow boxes show ablation craters. Total dose: 2.1 J = 0.35 W × 6 s
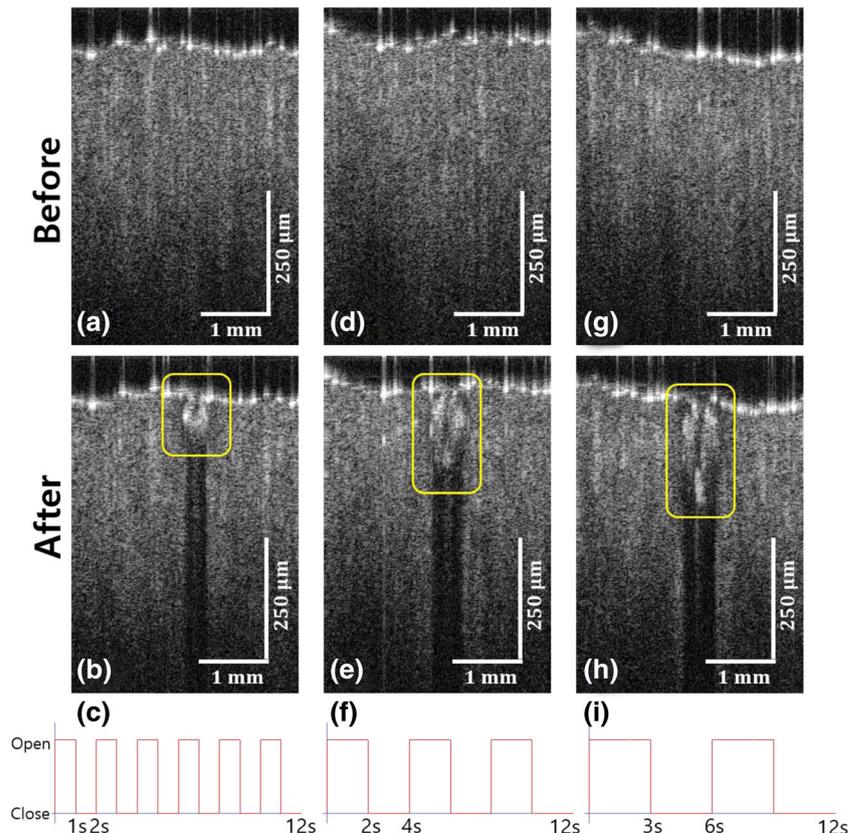
Images of porcine skin were relatively flat; however, it was difficult to obtain flat images of the hairless mouse because of its breathing movements and its small and wrinkled body. All experiments were performed three times with various conditions in each sample. One of the three ablation measurements was evaluated in Figs. 3, 4, and 5.

Influence of the duration per laser exposure on ablation

Shutter on-off frequency modulation was varied to determine whether there was a correlation between ablation and the laser exposure conditions. To generate various laser exposure conditions, a customized external shutter was set in the beam path. The shutter was controlled by the MCU through customized firmware. Figure 3 shows images of the in vitro experiments. The modulated pulses in [Fig. 3(c), (f), (i)] reflect open and closed shutters modulating the laser exposure conditions; in other words, the images show concurrence between shutter pulses and laser exposure conditions. The craters shown in [Fig. 3(b), (e), (h)] had different depths and widths despite application of the same irradiation conditions, except for the duration per laser exposure. The total shutter-open time (6 s)

and shutter-close time (6 s) were the same. After laser ablation with each condition for 12 s, experiments with various laser exposures demonstrated that shorter exposures generate shallower craters than longer exposures. These tests were repeated using the hairless mouse under anesthesia. The main difference between the mouse model and the porcine skin model was the production of chromophores to reduce contraction in ablation because of the thin skin of the hairless mouse. Upon laser irradiation until ablation was generated, radical contractions of skin brought movement beyond the range limits of OCT. Therefore, a black water–based pen was painted on the skin to accelerate ablation for acquisition of images in the tests modulating duration per laser exposure. Results are shown in Fig. 4.

Ablation experiments using the hairless mouse were performed using the same concept except chromophores. The total shutter-open time (1 s) and shutter-close time (1 s) were the same. The ablation craters shown in [Fig. 4(b), (e), (h)] are different sizes, consistent with the porcine skin results. Ablation with longer exposures caused deeper craters than shorter exposures. These results confirmed the correlation between ablation and the duration per laser exposure in in vivo and in vitro experiments.

Fig. 4 Ablation results for a hairless mouse obtained by modulating the duration per laser exposure. (a, d, and g) Images of the samples before laser irradiation. Each ablation was performed for a total of 1 s. The duration in each period for (a and b) was 0.05 s. The duration in each period for (d and e) was 0.1 s. The duration in each period for (g and h) was 0.5 s. The duty cycles of all periods were 50%. Laser beam power was 570 mW. The yellow boxes show ablation craters. Total dose: 0.235 J = 0.57 W × 0.5 s
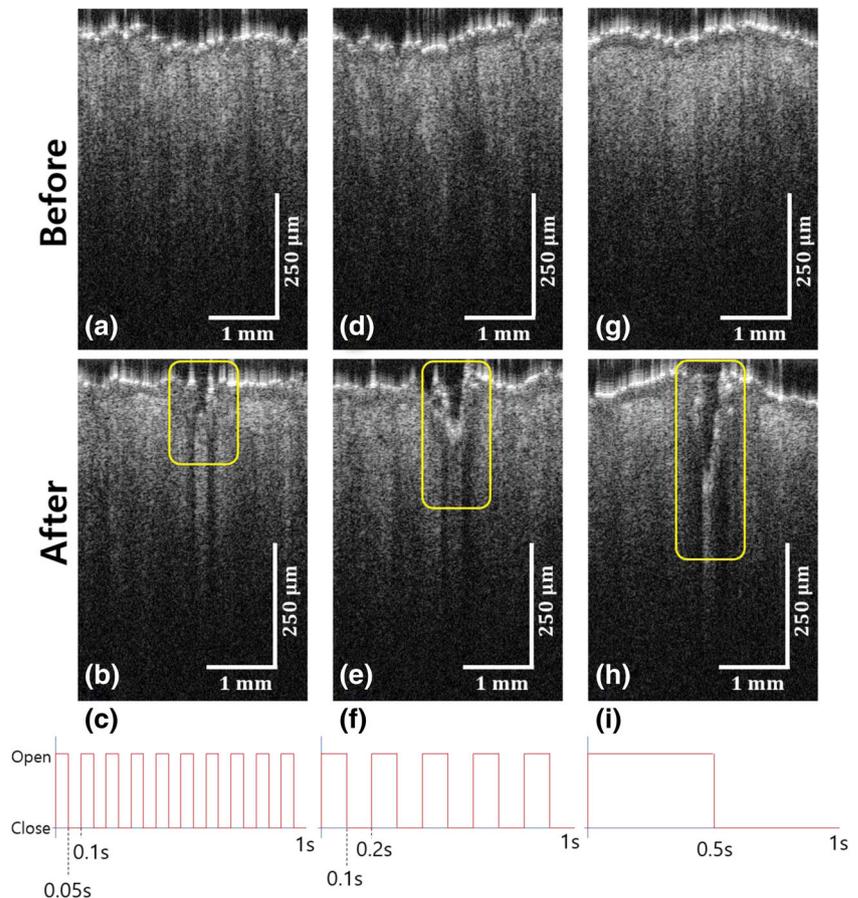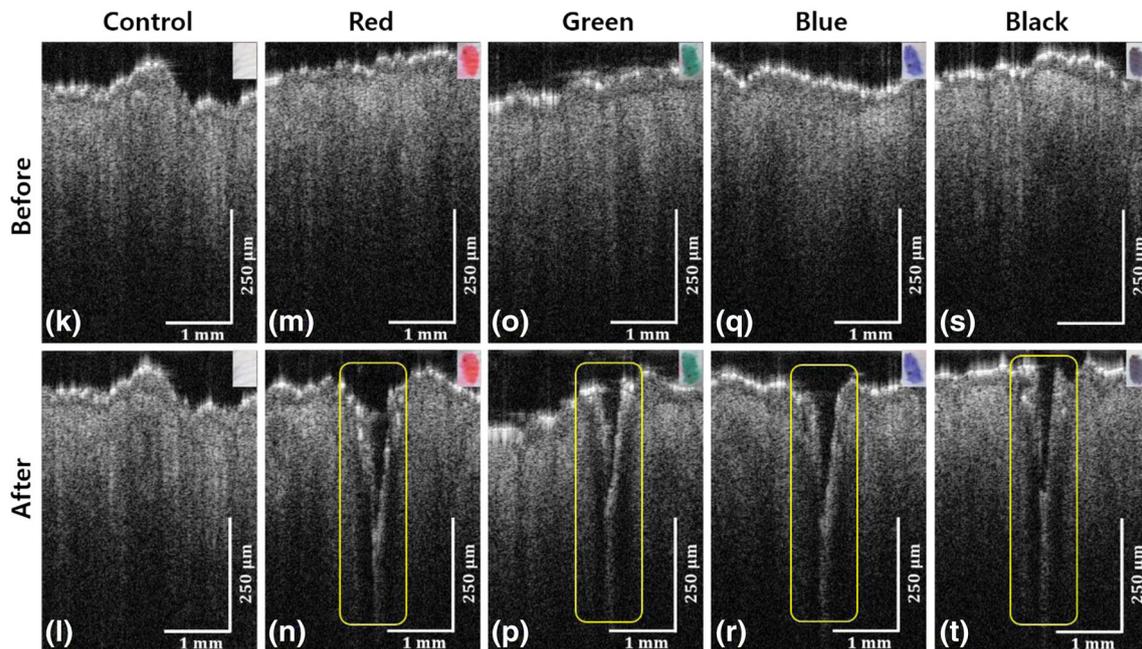
Porcine skin
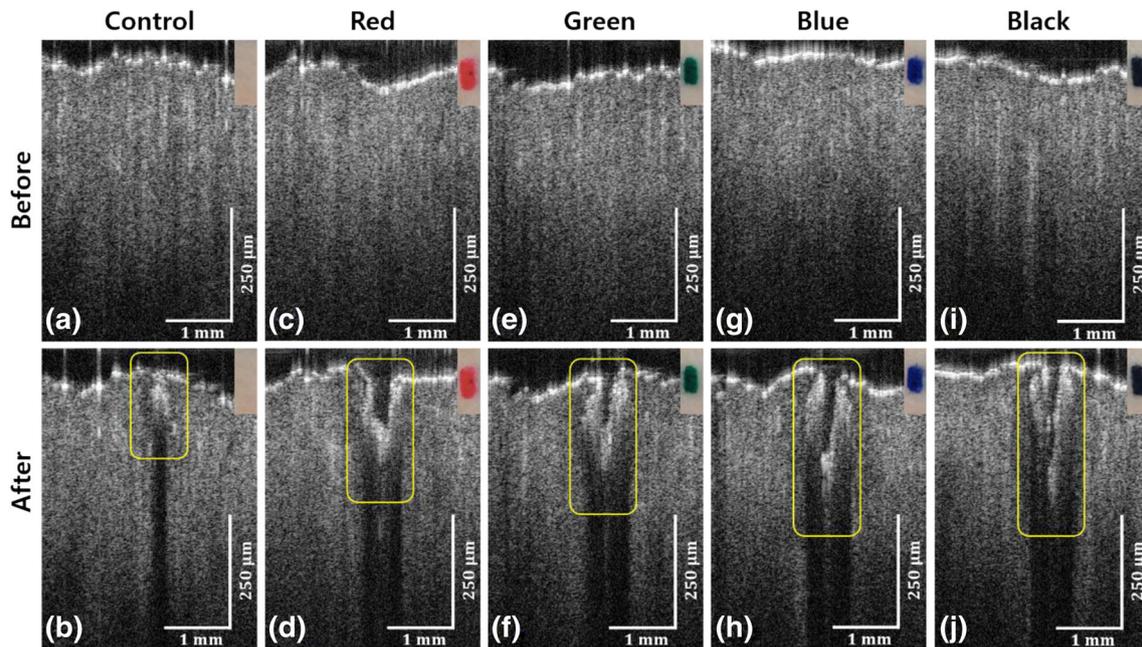
Hairless mouse skin

Fig. 5 Ablation results for porcine skin and hairless mouse skin painted with four colors. (**a**), (**c**), (**e**), (**g**), (**i**), (**k**), (**m**), (**o**), (**q**), and (**s**) Images of the samples before operating the laser. (**a**, **b**) and (**k**, **l**) Control group without treatment. (**c**, **d**) and (**m**, **n**), (**e**, **f**) and (**o**, **p**), (**g**, **h**) and (**q**, **r**), and (**i**, **j**) and (**s**, **t**) treated with red, green, blue, and black dyes, respectively. The experiments with porcine skin were performed at 525 mW for 1 s and the experiments with hairless mouse were used at 571 mW for 1 s. The yellow boxes show ablation craters. Total dose of irradiated laser on porcine skin: 0.525 J = 0.525 W × 1 s and hairless mouse: 0.571 J = 0.571 W × 1 s

Ablation of various chromophores

Ablation efficiency is dependent on the irradiation conditions and energy absorption of the laser. In initial experiments, the

laser conditions were modulated; therefore, in our next experiments, we focused on modulating the absorption of laser energy. To create absorbing elements, water-based ink was painted on the surface of samples as a chromophore. None

of the components of the pens except the dye had any influence on ablation. Experimental samples were painted with four colors: red, green, blue, and black. Figure 5 shows the results obtained for the colored samples.

After laser irradiation, all targets shown in Figs. 5 were ablated. In repeated experiments, small damage zones and no changes were observed in the control group [Fig .5(a, b), (k, l)], whereas considerable changes, such as craters and peripheral contraction, were observed in experimental groups [Fig. 5(c, d), (e, f), (g, h), (i, j), (m, n), (o, p), (q, r), (s, t)]. However, the amount of ablation was not fixed for a given color type, because ablation was performed at the different locations. Different irradiation locations could influence ablation due to changes in absorption. Absorption could be changed by absorption spectra, components of tissue samples, absorptivity as a property of the colorant, and the mass of water-based pens. Comparing the hairless mouse and porcine skin samples, the control for the hairless mouse [Fig. 5(k, l)] showed less damage than the control for the porcine skin [Fig. 5(a, b); however, an opposite trend was observed for the experimental groups. These results are attributable to differences in the tone, thickness, and composition of porcine and hairless mouse skin. Although differences and correlations according to various colors were not fixed because of the various elements, there were considerable differences between the non-colored control and colored groups.

Discussion

The objective of this study was to investigate laser ablation differences in the tissue according to modulated duration per laser exposure and colored chromophores on the skin of animal models. We demonstrated that modulated laser duration decrease the thermal damage at the illuminated laser craters as well as painted chromophores on the target increase the laser absorption efficiency through deepening crater depths. Laser irradiation could generate heat deposition in the tissue causing post-inflammatory hypopigmentation and hyperpigmentation (PIH) or scar. The PIH was one of side effects after laser treatment leading to hyper- or hypo-pigmented macules. Our demonstrated methods could hold the potential to develop

Table 2 Depths of craters caused by 1-s ablation of the porcine skin surface

Laser power (W, Watt)	Depth (μm) of craters by types of chromophores				
	Control	Red	Green	Blue	Black
0.525	0	75.03	119.31	159.90	191.88
0.600	0	109.47	131.61	132.84	136.53
1.000	0	174.66	217.71	167.28	175.89

Table 3 Depths of craters caused by 1-s ablation of the hairless mouse skin surface

Laser power (W, Watt)	Depth (μm) of craters by types of chromophores				
	Control	Red	Green	Blue	Black
0.571	0	320.80	243.54	270.60	255.84
0.640	0	308.73	319.80	382.53	279.21
1.000	0	355.47	344.40	418.20	440.34

optimal laser treatment protocols for safe and efficient tissue treatment.

We compared the depth of craters between non-colored controls and colored experimental groups. In Tables 2 and 3, all colored samples were ablated but of different depths as a result of different irradiation locations with different properties including tone, thickness, and skin composition. Although no craters were observed in the non-colored control in either porcine skin or hairless mouse skin, slight changes were observed in porcine skin because porcine skin was darker in color than hairless mouse skin. These results indicate that the presence of color increases laser absorption in the tissue. In particular, our results demonstrate that thinly colored the skin can increase ablation efficiency without dyeing the cells or the tissue.

Colors were painted on the skin of hairless mouse in all the experiments except (k and l) of Fig. 5. Black color was used in the experiments for shutter on-off frequency modulation to enhance absorption efficiency because only skin contractions without ablation were observed in non-colored hairless mouse with shutter on-off frequency modulation. Although samples in both experiments were irradiated for 1 s, craters could be not detected in the control in Fig. 5(k, l).

Conclusions

In this research, we investigated the effects of duration modulation of laser exposure and different chromophores on the target. Coloring chromophores with water-based dyes using pens increased tissue damage without dyeing cells or tissue. This research can be applied to dermatologic treatments and brain surgery with laser irradiation. In dermatology, colored chromophores on the tissue could help remove pigmentation with low-energy lasers as well as minimize peripheral damage on the pigmentation area. In order to develop appropriate standards for laser treatment, differences in absorption related to skin tone and pigmentation variation should be considered. Future experiments will investigate correlations between skin tone and absorption efficiency using phantoms. Research with new skin phantoms could demonstrate the relationship between chromophores and absorption efficiency in laser

treatment. This can be applied in various surgical procedures as well as in normal skin treatments that require a low-energy laser beam as well as precise control of medical probes.

Compliance with ethical standards

Experiments using hairless mouse were approved by the institutional animal care and use committee (IACUC) of Dankook University.

Conflicts of interest   The authors declare that they have no conflict of interest.

References

1. Studdert V. P, Gay CC, Blood DC (2007) Saunders comprehensive veterinary dictionary 3rd. Saunders Elsevier, St. Louis, Missouri, USA

2. Gower MC (2000) Industrial applications of laser micromachining. Opt Express 7(2):56–67. https://doi.org/10.1364/OE.7.000056

3. Cutroneo M, Torrisi L, Seolaro C (2010) Laser applications in bio-medical field

4. Ohmi M, Tanizawa M, Fukunaga A, Haruna M (2005) In-situ observation of tissue laser ablation using optical coherence tomography. Opt Quant Electron 37(13–15):1175–1183. https://doi.org/10.1007/s11082-005-4189-2

5. Hsieh YS, Ho YC, Lee SY, Chuang CC, Tsai J, Lin KF, Sun CW (2013) Dental optical coherence tomography. Sensors 13(7):8928–8949. https://doi.org/10.3390/s130708928

6. Vogl TJ, Eichler K, Mack MG, Zangos S, Herzog C, Thalhmmer A, Englemann K (2004) Interstitial photodynamic laser therapy in interventional oncology. Eur Radiol 14(6):1063–1073. https://doi.org/10.1007/s00330-004-2290-8

7. Liao H, Fujiwara K, Ando T, Maruyama T, Kobayashi E, Muragaki Y, Iseki H, Sakuma I (2013) Automatic laser scanning ablation system for high-precision treatment of brain tumors. Lasers Med Sci 28:891–900. https://doi.org/10.1007/s10103-012-1164-6

8. Ngoi BKA, Hou DX, Koh LHK, Hoh ST (2005) Femtosecond laser for glaucoma treatment: a study on ablation energy in pig iris. Lasers Med Sci 19:218–222. https://doi.org/10.1007/s10103-004-0323-9

9. Mir M, Meister J, Franzen R, Sabounchi SS, Lampert F, Gutknecht N (2008) Influence of water-layer thickness on Er:YAG laser ablation of enamel of bovine anterior teeth. Lasers Med Sci 23:451–457. https://doi.org/10.1007/s10103-007-0508-0

10. Beier C, Kaufmann R (1999) Efficacy of erbium:YAG laser ablation in darier disease and Hailey Hailey disease. Arch Dermatol 135(4):423–427. https://doi.org/10.1001/archderm.135.4.423

11. Kuperman-Beade M, Levine VJ, Ashinoff R (2001) Laser removal of tattoos. Am J Clin Dermatol 2(1):21–25. https://doi.org/10.1177/039463201202500226

12. Walsh JT, Flotte TJ, Deutsch TF (1989) Er:YAG laser ablation of tissue : effect of pulse duration and tissue type on thermal damage. Lasers Surg Med 9(4):314–326. https://doi.org/10.1002/lsm.1900090403

13. Walsh JT, Flotte TJ, Anderson RR, Deutsch TF (1988) Pulsed CO_2 laser tissue ablation: effect of tissue type and pulse duration on thermal damage. Lasers Surg Med 8(2):108–118. https://doi.org/10.1002/lsm.1900080204

14. Walsh JT, Deutsch TF (1988) Pulsed CO2 laser tissue ablation: measurement of the ablation rate. Laser Surg Med 8(3):264–275. https://doi.org/10.1002/lsm.1900080308

15. Cummings JP, Walsh JT (1993) Tissue tearing caused by pulsed laser induced ablation pressure. Appl Opt 32(4):494–503. https://doi.org/10.1364/AO.32.000494

16. Walsh JT, Van Leeuwen TG, Jansen ED, Motamedi M, Welch AJ (2011) Pulsed laser tissue interaction. In: Welch A, van Gemert M (eds) Optical-thermal response of laser-irradiated tissue. Springer, Dordrecht, pp 617–649

17. Kang HW, Kim JH, Steven PY (2013) In vitro investigation of wavelength-dependent tissue ablation: laser prostatectomy between 532nm and 2,01um. Lasers Surg Med 42(3):237–244. https://doi.org/10.1007/s10103-012-1235-8

18. Huang Y, Jivraj J, Zhou J, Ramjist J, Wong R, Gu X, Yang VX (2016) Pulsed and CW adjustable 1942nm single-mode all-fiber Tm-doped fiber laser system for surgical laser soft tissue ablation applications. Opt Express 24(15):11674–11686. https://doi.org/10.1364/OE.24.016674

19. Steiner R, Kunzi-Rapp K, Scharffetter-Kochanek K (2003) Optical coherence tomography: clinical applications in dermatology. Med Laser Appl 18(3):249–259. https://doi.org/10.1078/1615-1615-00107

20. Fercher AF, Drexler W, Hitzenberger CK, Lasser T (2003) Optical coherence tomography-principles and applications. Rep Prog Phys 66(2):239–303. https://doi.org/10.1088/0034-4885/66/2/204

21. Kim BK, Kim DY (2016) Enhanced tissue ablation efficiency with a mid-infrared nonlinear frequency conversion laser system and tissue interaction monitoring using optical coherence tomography. Sensors 16(5):598. https://doi.org/10.3390/s16050598

22. Wisweh H, Merkel U, Hüller A, Lüerßen K, Lubatschowski H (2007) Optical coherence tomography monitoring of vocal fold femtosecond laser microsurgery. Therapeutic Laser Applications and Laser-Tissue Interactions III Vol 6632_6 of Proceedings of SPIE-OSA Biomedical Optics https://doi.org/10.1364/ECBO.2007.6632_6

23. Kim DY, Fingler J, Zawadzki RJ, Park SS, Morse LS, Schwartz DM, Fraser SE, Werner JS (2012) Noninvasive imaging of the foveal avascular zone with high-speed, phase-variance optical coherence tomography. Invest Ophthalmol Vis Sci 53(1):85–92. https://doi.org/10.1167/iovs.11-8249

24. Kim DY, Werner JS, Zawadzki RJ (2012) Complex conjugated artifact-free adaptive optics optical coherence tomography of in vivo human optic nerve head. J Biomed Opt 17(12):126005. https://doi.org/10.1117/1.JBO.17.12.126005

25. Kim DY, Fingler J, Zawadzki RJ, Park SS, Morse LS, Schwartz DM, Fraser SE, Werner JS (2013) Optical imaging of the chorioretinal vasculature in the living human eye. PNAS 110(35): 14354–14359. https://doi.org/10.1073/pnas.1307315110

26. Cho NH, Park KB, Wijesinghe RE, Shin YS, Jung WG, Kim JH (2014) Development of real-time dual-display handheld and bench-top hybrid-mode SD-OCTs. Sensors 14(2):2171–2181. https://doi.org/10.3390/s140202171

27. Wessels R, De Bruin DM, Faber DJ, Van Leeuwen TG, Van Beurden M, Ruers TJM (2014) Optical biopsy of epithelial cancers by optical coherence tomography (OCT). Lasers Med Sci 29:1297–1305. https://doi.org/10.1007/s10103-013-1291-8

28. Cho NH, Lee SH, Jung W, Jang JH, Kim J (2015) Optical coherence tomography for the diagnosis and evaluation of human otitis media. J Korean Med Sci 30(3):328–335. https://doi.org/10.3346/jkms.2015.30.3.328

29. Murphy MJ, Torstensson PA (2014) Thermal relaxation times: an outdated concept in photothermal treatments. Lasers Med Sci 29(3):973–978. https://doi.org/10.1007/s10103-013-1445-8

30. Yadav RK (2009) Definitions in laser technology. J Cutan Aesthet Surg 2(1):45–46. https://doi.org/10.4103/0974-2077.53103

31. Hamblin MR, Demidova TN (2006) Mechanisms of low level light therapy. Proc SPIE 6140:614001. https://doi.org/10.1117/12.646294

32. Jacobi U, Kaiser M, Toll R, Mangelsdorf S, Audring H, Otberg N, Sterry W, Lademann J (2007) Porcine ear skin: an in vitro model for human skin. Skin Res Technol 13(1):19–24. https://doi.org/10.1111/j.1600-0846.2006.00179.x